Robust design optimisation of underplatform dampers for turbine applications using a surrogate model

Ye Yuan[1]*, A. Jones[2], R. Setchfield[2], C.W. Schwingshackl[1]

[1] *Department of Mechanical Engineering, Imperial College London, Exhibition Road, London SW7 2AZ, UK*

[2] *Rolls-Royce plc, Derby DE2 48J, UK*

Abstract

Underplatform dampers (UPD) represent an effective way to limit blade vibration in turbomachinery via frictional energy dissipation, leading to a wide range of applications. The design of an effective and reliable UPD is highly challenging, due to the inherently nonlinear nature of the contact forces, the associated computational cost for high fidelity simulation, and the manufacturing uncertainties in damper geometry. This paper presents a novel UPD optimisation approach that combines high-order, detailed nonlinear modelling of the damper interfaces with a surrogate model optimisation technique. The nonlinear dynamic behaviour of the UPD is predicted using the existing explicit damper model in combination with an 'in-house' multi-harmonic balance solvers, which enables capture of the damper kinematics and local contact conditions. A radial basis function based surrogate model will be used to address the computational requirement of the high fidelity simulations for alternative designs. The objective function takes into account the damping performance, resonance frequency stability and robustness due to possible uncertain variations of design parameters with manufacture tolerance. The feasibility of the proposed approach is demonstrated on a cottage roof UPD by comparing the proposed optimisation method with conventional parametric simulation method. A significantly improved solution with considerable reduction in computational effort is achieved by the current method.

Keywords: Surrogate model optimisation, Underplatform damper, Nonlinear dynamics, Turbine blade vibration

1. Introduction

The optimisation of underplatform dampers (UPD) has been receiving growing interest in recent publications, see [1, 2]. The UPD is an established passive friction device that

*Corresponding author
Email address: ucemyyu@ucl.ac.uk (Ye Yuan[1])

mitigates the threat of high-cycle fatigue for gas turbine blades due to large resonance stresses [3]. This is achieved by reducing the resonance amplitude via frictional damping between adjacent blades [4]. The main design criterion is an optimal damper geometry that provides a maximum reduction of resonance amplitudes [5]. Due to the frictional nature of the problem, the dynamic response of a bladed disc with UPD is strongly nonlinear, and the UPD performance can be very sensitive to its interface geometry [6], often leading to a large variability in damper performance. Consequently the UPD design requires high-order nonlinear dynamic simulations of the blade-damper system to capture the nonlinear behaviour at the blade-damper interface, characterised by transitions between stick, slip, and separation. A range of high-order approaches have been developed over the years to predict the nonlinear dynamic behaviour of an UPD accurately [6–14] based on state-of-the-art strategies, such as component mode synthesis [15], multi harmonic balance [16] and reduced order modelling [17]. The results of these approaches show good agreement with experimental data, but they come at a very high computational cost due to large number of degrees of freedom needed to characterise the vibrational behaviour. This poses a significant challenge for the optimal design of UPD which can require a large range of design iterations due to the nonlinear nature of the problem.

The widely adopted approach for optimisation studies of UPD designs is based on sensitivity analysis (or known as parametric simulation method [18]) of the forced resonance responses to a finite number of variations of the design parameters. The parametric simulation method varies the input of each variable to investigate the sensitivity on the design objectives while all the other variables are kept unchanged. As a result an *optimal* design can only be obtained after this procedure is repeated for all variables of interest, leading to a computationally expensive process. Focusing on the optimal non-geometric design parameters, Petrov [4, 19] and Krack el al. [20] carried out sensitivity analysis of UPD design to the contact parameters at the blade-damper interface, and uncertainties in the damping and excitation parameters, respectively. Taking into consideration the geometry change during the optimisation process, Tang and Epureanu [21] carried out a parametric study on the effectiveness of a V-shaped friction ring damper using a reduced order modelling method. They investigated the sensitivity of frequency split (between sliding and sticking frequencies) by simultaneously varying two (out of four) geometric parameters at the same time. Considering the effect of asymmetric platform angles, Panning et al. [22] investigated the influence of contact geometry on damping effectiveness by parametrically varying both the geometry of blade platform and damper.

It is well-known that the parametric simulation method is not efficient at finding the optimal and can be time-consuming, since only partial improvement in the solution is available from each repetition of parametric simulation. An alternative approach is to carry out ‘simulation-based optimisation’, which is commonly used for ‘black-box’ optimisation problems where analytical solutions and derivatives of variables are unknown [23]. During simulation-based optimisation, automated objective function evaluation and subsequent adjustment of UPD parameters according to an optimisation algorithm are carried out in a loop manner to progressively approximate to a ‘solution’ (optimal or near the optimal) that satisfies an optimality condition in the search space. Conventional optimisation algorithms – for example gradient based (e.g. conjugate-gradient, quasi-Newton and sequential quadratic programming), derivative-free (e,g, Nelder-Mead and pattern search), genetic algorithms and particle swarm as reviewed in [24] – require a large number of function evaluations that make them unsuitable for the current problem which has a computationally expensive objective function.

Recently, there has been growing interest in using surrogate model based algorithms to address computationally expensive simulation-based optimisation problems [25–30]. A surrogate model has the advantage of yielding a satisfactory solution with relative few function evaluations since it is a computationally cheap approximation of the expensive objective functions evaluated at sample points, which is used to guide the search for improved solutions at untried points/configurations. The key contributing factor to the surrogate models' efficiency and affordability is that, instead of pursuing accuracy over the entire design space, the surrogate predictions become more accurate in the region of interest as the search progresses [31]. Surrogate models can be either non-interpolating (for example polynomial regression models [32] and multivariate adaptive regression splines [33]) or interpolating (for example Radial basis functions [34] and Kriging [35]).

The objective of this paper is to develop a methodology for UPD design optimisation, leading to an excellent and robust damping performance. The novel approach will be based on high-order modelling of the contact interfaces, in combination with a surrogate model to optimise the geometric configuration of the UPD. The objective function takes into account the variations of geometric configuration due to manufacture tolerance, which could significantly alters the dynamic behaviour of the blade as will be shown in section 4. This paper can be regarded as a *proof-of-concept* study which only deals with a few geometric design parameters to a cottage-roof-damper. The proposed methodology is transferable for other types of dampers (e.g. cylindrical, asymmetrical and ring) and can include additional geometric and non-geometric (e.g. contact and loading) parameters.

2. UPD modelling

The nonlinear dynamic analysis of the UPD is based on the explicit damper modelling approach recently developed by Pesaresi et al. [6]. This method has the following features: (1) it incorporates detailed three-dimensional finite element modelling of the blades and damper; (2) it considers detailed nonlinear representation of the interface with realistic contact pressures; and (3) it uses a Multi Harmonic Balance Solver to carry out the nonlinear dynamic analysis capturing both the overall dynamic response and local contact conditions during vibration. Validation of the explicit damper modelling approach was provided in [6] and consequently a short description of the methodology will be provided in this section to facilitate the understanding of this research work.

2.1. UPD geometric parametrisation and uncertainty quantification

Figure 1 shows the academic UPD test rig at Imperial College London [6], which will be the test case for this study. It consists of two blades with platforms on each side, and a

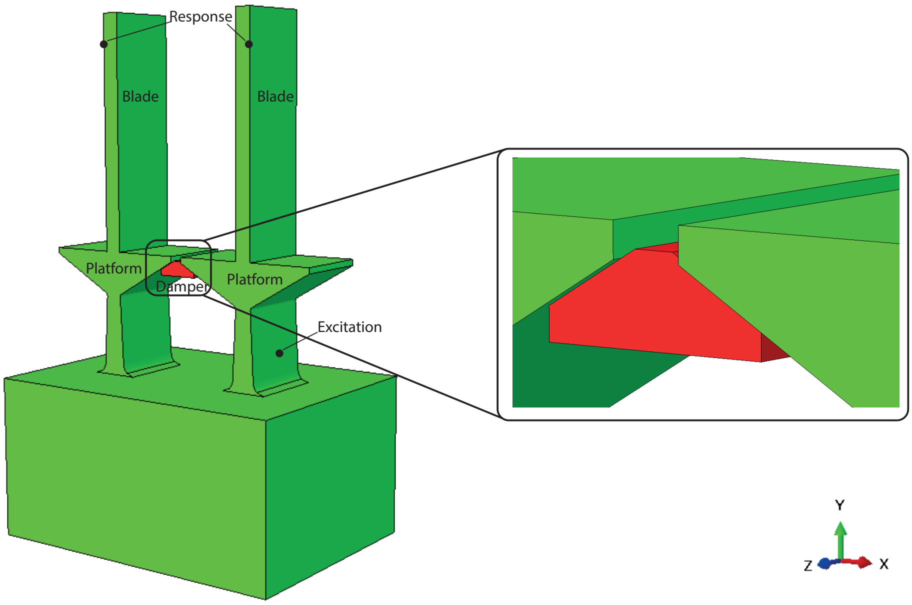

Figure 1: Three-dimensional blade-damper system developed in [6]: two blades and platforms (green) in contact with a cottage-roof damper (red).

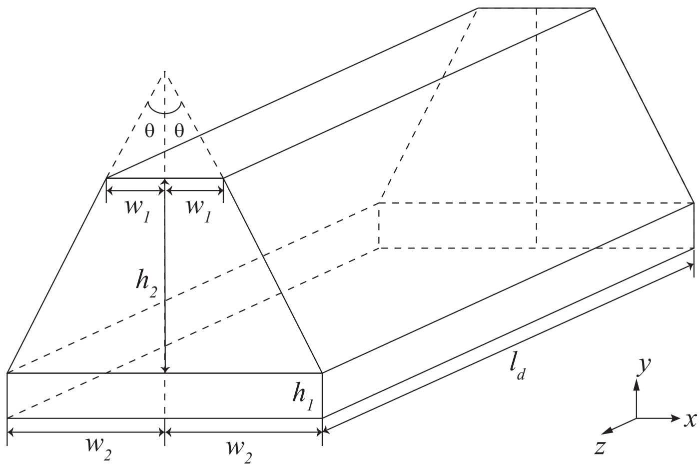

Figure 2: Schematic of the three-dimensional cottage-roof damper design.

cottage-roof damper that sits between the two blades. The three-dimensional schematic of the cottage-roof damper can be seen in Fig. 2. The geometry of the damper can be characterised by the following parameters: w_1 and w_2 - half of the upper and lower damper width; h_1 - the height of the base; h_2 - the height of the trapezium; θ - half of the damper groove angle; and l_d - the damper length. In this study, a constant h_1=2.8 mm and l_d=38 mm will be assumed, identical to those in [6], while w_2, h_2 and θ will be available for design optimisation. The remaining parameter, w_1, can be calculated as follows,

$$w_1 = w_2 - \tan(\theta)h_2. \tag{1}$$

In this study, the design parameters are expressed in non-dimensional forms:

$$\bar{w} = \frac{w_2}{w_0}, \quad \bar{\theta} = \frac{\theta}{\theta_0}, \quad \bar{h} = \frac{h_2}{h_0} \tag{2}$$

where the reference values, w_0=10.24 mm, h_0=4.88 mm and θ_0=60° represent the original design in [6]. Geometrical constraints (i.e. $w_1 > 0$ and $\theta < 90°$) dictate the following inequality relationships to ensure realistic damper geometries:

$$\bar{w}w_0 - \tan(\bar{\theta}\theta_0)\bar{h}h_0 > 0 \quad \text{and} \quad \bar{\theta} < 1.5. \tag{3}$$

It should be noted that UPD's volume, and its mass, would not be conserved according to the above parameterisation. This, however, would not affect the outcome of the current optimisation study since the effect of geometrical and mass variation upon the damper's kinematics, the modal properties, and the static pre-load distribution due to varying centrifugal force would be captured by the aforementioned high-fidelity modelling approach [6].

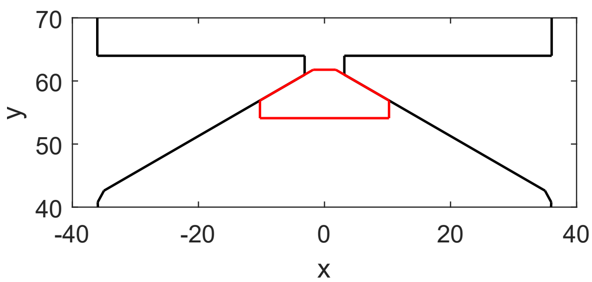

(a) $\bar{\theta} = 1$, $\bar{w} = 1$ and $\bar{h} = 1$

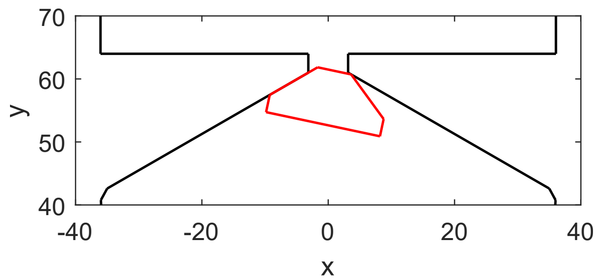

(b) $\bar{\theta} = 0.8$, $\bar{w} = 0.9$ and $\bar{h} = 1.2$

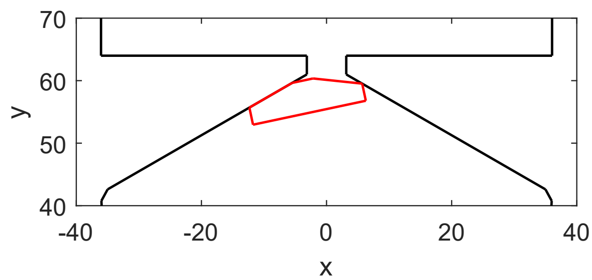

(c) $\bar{\theta} = 1.2$, $\bar{w} = 0.9$ and $\bar{h} = 0.5$

Figure 3: Examples of different UPD designs based on current parametrisation.

Figure 3 shows three examples of UPD designs generated by the proposed geometric parametrisation. The contact condition at the interface between platform and damper depends upon the value of $\bar{\theta}$. When $\bar{\theta} = 1$ (see Fig. 3a) both surfaces of damper are in full contact with the platform, whereas when $\bar{\theta} \neq 1$ the entire left surface of the damper conforms to that of the platform and the other side is in line contact at either the upper (see Fig. 3b), or lower (see Fig. 3c) part of the damper. It is assumed in this study that under centrifugal force the damper will rotate (in $x - y$ plane) and eventually settles to a final position with one surface in full contact. The impact of this assumption was considered negligible, since it can be assumed that imperfection due to asymmetries in the manufactured damper or platforms most likely will lead to such a configuration during operation. The detailed process of settling to the final position is neglected in this study since the current nonlinear dynamic solver cannot capture large motion of the damper before the damper-blade system is in full contact. Nevertheless, the small-scale rolling motion of the damper during the vibration cycle will be captured by the nonlinear solver since the nonlinear elements can separate during a vibration cycle, leading to a potential rotation of the damper [6]. Due to the symmetry of the UPD design, all configurations with $\bar{\theta} \neq 1$ will be rotated, clockwise, and translated such that the left slope is adhered to the left platform and right counterpart is in contact with the right platform.

There exist statistical uncertainty quantification methods (e.g. Monte Carlo simulation [36] and polynomial chaos expansions [37]) to quantify variability of design parameters due to manufacture variability. But they demand thousands of analyses of deterministic models which make them unfeasible for the current computationally expensive problem. Instead, a nominal configuration was defined ($\bar{\theta}$, $\bar{w}$, $\bar{h}$), from which worst case variations for a minimum ($\bar{\theta} - \Delta\bar{\theta}$) and maximum ($\bar{\theta} + \Delta\bar{\theta}$) half groove angle were defined, leading to two additional geometries for each damper design with $\bar{\theta} + \Delta\bar{\theta}$, $\bar{w}$, $\bar{h}$ and $\bar{\theta} - \Delta\bar{\theta}$, $\bar{w}$, $\bar{h}$. To keep the number of variations to a minimum for this proof of concept study, it was assumed that both the non-dimensional width $\bar{w}$ and height $\bar{h}$ are unaffected by the manufacturing process.

2.2. nonlinear dynamic analysis

Figure 4 shows the steps required to calculate the nonlinear frequency response function (FRF) for a given input geometry - this can be either the nominal ($\bar{\theta}$, $\bar{w}$, $\bar{h}$) or variational configurations ($\bar{\theta} + \Delta\bar{\theta}$, $\bar{w}$, $\bar{h}$ and $\bar{\theta} - \Delta\bar{\theta}$, $\bar{w}$, $\bar{h}$) as defined in section 2.1. It is worth mentioning that the steps shown here are automated using a MATLAB code, the process of which is indispensable to facilitate the evaluation of alternative geometry configurations within the optimisation loop (to be presented in section 3). The blade-damper system is discretised with 13632 8-noded brick elements, which is shown to be sufficient from results of convergence studies. Special care is taken to ensure that nodes of the platform and damper meshes are coincident at the interface, see Fig. 5 for an example. This is followed by detailed three-dimensional (3D) finite element simulations for the blade-damper system (see Fig. 1). Modal analysis and quasi-static nonlinear contact analysis, will be carried out separately to obtain the linear dynamic response of the system and the initial pre-load distribution σ_0 at the interface respectively. The blade-damper system is struck by a harmonic excitation load at a location below the platform and the response near the tips of the blades is extracted, as seen in Fig. 1. The base of the blade-damper system is fully clamped.

The damper-platform interface is discretised with a grid of three-dimensional (3D) nonlinear

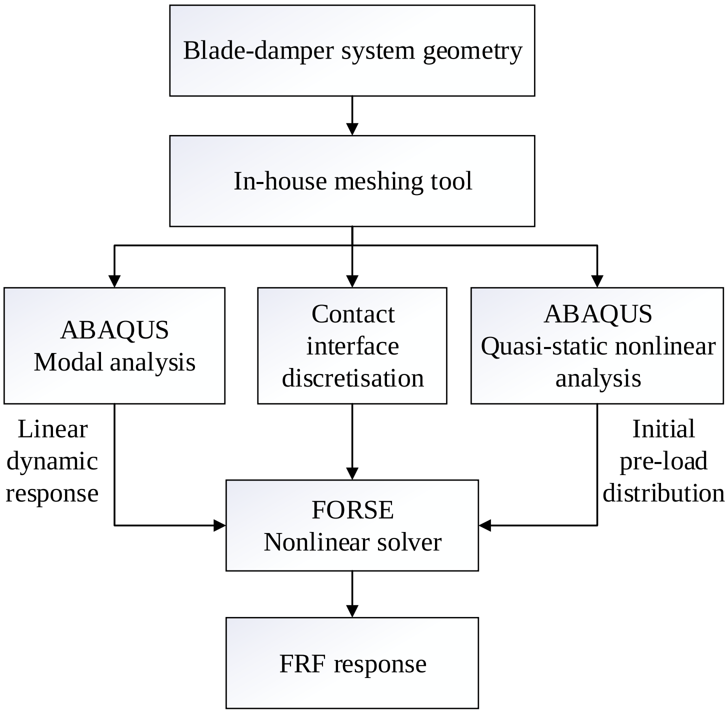

Figure 4: Automated process to carry out the nonlinear dynamic analysis from a given set of design parameters.

contact elements, based on two decoupled Jenkins elements [38], as shown in Fig. 5. The nonlinear element allows capturing in-plane stick-slip motion, and out-of-plane separation during a vibration cycle, and leading to an accurate representation of the contact mechanism during vibration. The contact properties for the nonlinear element are characterised by the friction coefficient μ, the initial pre-load σ_0 and the tangential K_t and normal K_n stiffness, and can be obtained experimentally [39, 40].

The equation of motion for the blades and damper (i.e. contact nodes on the interface and selected nodes of blade, platform and damper) can be written as follows:

$$\mathbf{M}\ddot{\mathbf{y}}(t) + \mathbf{C}\dot{\mathbf{y}}(t) + \mathbf{K}\mathbf{y}(t) + \mathbf{F}_{nl}(\dot{\mathbf{y}}(t), \mathbf{y}(t)) = \mathbf{P}(t) \tag{4}$$

where $\mathbf{M}$, $\mathbf{C}$ and $\mathbf{K}$ are the mass, damping and stiffness matrices; $\mathbf{P}$ are the external excitation forces; and $\mathbf{F}_{nl}$ are the nonlinear forces acting at the interface. The equation of motion can be solved using the Multi Harmonic Balance Solver, FORSE (FOrced Response SuitE) [10, 17, 41, 42], which permits a fast and reliable computation of the resulting nonlinear frequency response function (FRF) for a given input geometry.

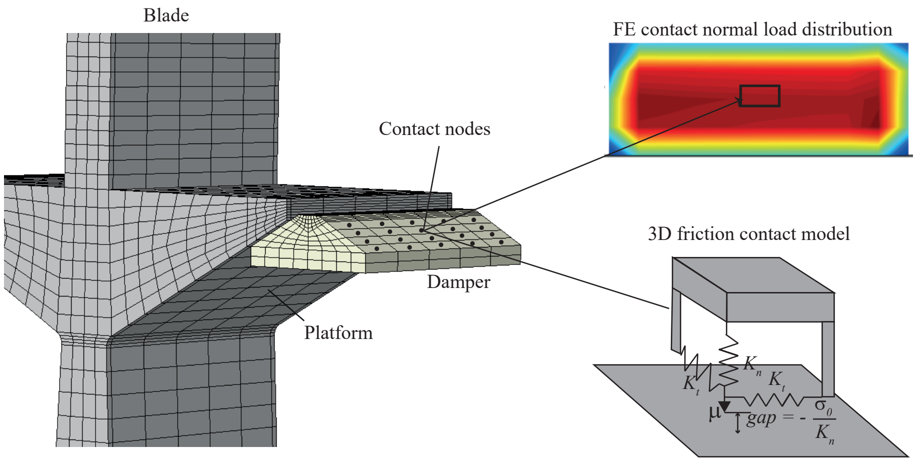

Figure 5: General scheme of the contact interface discretisation.

3. Optimisation

The current methodology combines the high-order detailed modelling approach and a surrogate model method to optimise the geometric configuration of the UPD. The surrogate model is highly suitable for the current problem due to its ability to emulate the expensive response of ‘black box’ simulation through construction of a cheap-to-evaluate surrogate model. The objective function targets good and robust damping performance as well as resonance frequency stability, independent of typical manufacturing tolerances. In this section only the key aspects of the implementation procedure for a surrogate model of the current nonlinear dynamic problem will be discussed, since a description of the the mathematical details of the approach are outside the scope of this study.

3.1. Surrogate model algorithm

Consider the following deterministic optimisation problem for UPD design characterised by the vector of design parameters $\mathbf{x} \in \mathbb{R}^{\mathbf{k}}$ and the resulting response behaviour (damping performance, robustness) $f(\mathbf{x}) \in \mathbb{R}$ as the optimisation target

$$\min_{\mathbf{x}}[f(\mathbf{x})] \tag{5a}$$

$$-\infty < x_i^l \leq x_i \leq x_i^u < \infty, \quad i = 1, ..., k, \tag{5b}$$

where x_i^l and x_i^u denote lower and upper variable bounds, respectively; k refers to the total number of design variables. The evaluation of objective function $f(\mathbf{x})$ for UPD will be presented in the next subsection. It should be noted here, that if the geometrical constraints (see Eq. 3) are violated, the objective function will not be evaluated due to infeasible damper geometry, and its value will be penalised to be a substantial value. Based on the surrogate model, the output of the simulation model (or true model) can be approximated as the sum of the surrogate model’s output $\hat{f}(\mathbf{x})$ and its error ϵ

$$f(\mathbf{x}) = \hat{f}(\mathbf{x}) + \epsilon. \tag{6}$$

The surrogate model algorithm iterates the following: gaining insights into f through discrete observations or samples, supervised learning that searches for a conceivable function $\hat{f}$ that would replicate observations of f, and enhancing the accuracy of $\hat{f}$ with further function calls.

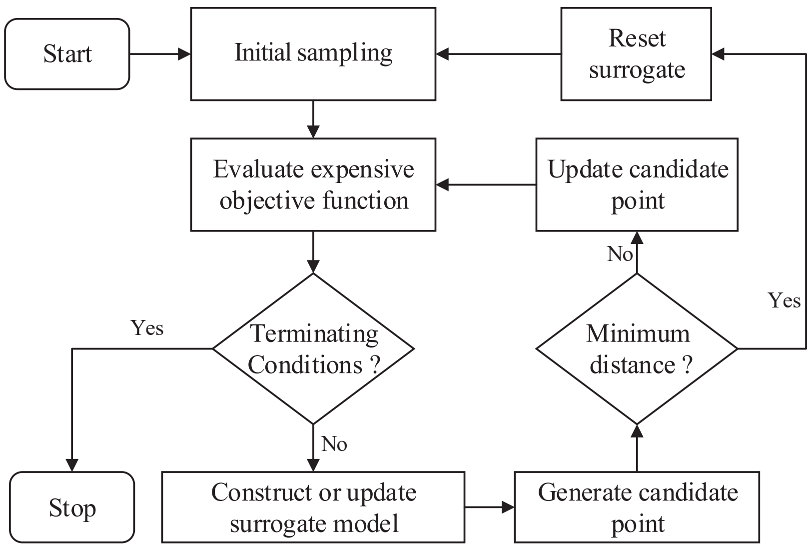

Figure 6: Flow-chart of the surrogate model algorithm.

Figure 6 shows the flow-chart to address this optimisation problem using a surrogate model algorithm. The algorithm comprises the following steps:

1. Evaluate the objective function $f(\mathbf{x})$ at q initial points of the domain according to a space-filling experimental design. Here, the initial points are taken from a quasi-random sequence (or known as low-discrepancy sequence) to achieve a reasonable uniformity. A commonly used sampling size of $q = 20$ [26] is adopted in this study.
2. This is followed by constructing the surrogate model by interpolating a radial basis function [34] through all of the already evaluated points (this could either be initial points or initial points together with candidate points). The data at which the objective function value is known (x_1, f_1),...,(x_n, f_n) are interpreted using the surrogate model expressed as follows

$$\hat{f}(x) = \sum_{\zeta=1}^{n} \lambda_\zeta \phi(||\mathbf{x} - x_\zeta||) + p(\mathbf{x}), \tag{7}$$

where $||\cdot||$ is the Euclidean norm; $\lambda_i \in \mathbb{R}$ are basis function weights; $p(\mathbf{x})$ denotes an optional polynomial tail of the form $\mathbf{b}^T\mathbf{x} + a$, $\mathbf{b} \in \mathbb{R}^k$, $a \in \mathbb{R}$. In this work, the cubic radial basis function $\phi(r) = r^3$ will be used following [43]. These unknown parameters are determined by solving the linear system [44]

$$\begin{bmatrix} \boldsymbol{\Phi} & \mathbf{P} \\ \mathbf{P}^T & 0 \end{bmatrix} \begin{bmatrix} \lambda \\ \mathbf{c} \end{bmatrix} = \begin{bmatrix} \mathbf{F} \\ \mathbf{0} \end{bmatrix}, \quad \text{where} \quad \mathbf{P} = \begin{bmatrix} \mathbf{x}_1^T & 1 \\ \mathbf{x}_2^T & 1 \\ \vdots & \vdots \\ \mathbf{x}_n^T & 1 \end{bmatrix}, \quad \lambda = \begin{bmatrix} \lambda_\mathbf{1} \\ \lambda_\mathbf{2} \\ \vdots \\ \lambda_\mathbf{n} \end{bmatrix} \quad \mathbf{c} = \begin{bmatrix} b_1 \\ b_2 \\ \vdots \\ b_k \\ a \end{bmatrix}, \quad \mathbf{F} = \begin{bmatrix} f_1 \\ f_2 \\ \vdots \\ f_n \end{bmatrix}, \tag{8}$$

and $\boldsymbol{\Phi}$ is an $n \times n$ matrix with entries $\Phi_{\zeta\nu} = \phi(||x_\zeta - x_\nu||)$, ζ, ν=1, ..., n. It is worth mentioning that while Eq. 7 is linear in terms of the basis function weights λ, yet the surrogate $\hat{f}$ can express a highly nonlinear response of the UPD.

3. The next function evaluation point, (referred to, hereafter, as *candidate point*), will be determined by minimising a merit function which balances minimising the surrogate $\hat{f}(\mathbf{x})$ and searching globally within the design space. The merit function $f_m(\mathbf{x})$ proposed by Regis and Shoemaker [43] is used here, which is a weighted combination of scaled surrogate and scaled distance:

$$f_m(\mathbf{x}) = w_m \frac{\hat{f}(\mathbf{x}) - \hat{f}_{\min}}{\hat{f}_{\max} - \hat{f}_{\min}} + (1 - w_m) \frac{d_{\max} - d(\mathbf{x})}{d_{\max} - d_{\min}}, \tag{9}$$

where $\hat{f}_{\max}$ and $\hat{f}_{\min}$ are maxima and minima surrogate value of $\hat{f}(\mathbf{x})$ obtained through evaluating thousands of pseudorandom vectors with scaled length to the point that has the smallest objective function value evaluated since the last surrogate reset; $d(\mathbf{x})$ is the minimum distance of the current point to the previous evaluated points (the points at which the objective function value is known), $d_{\max}$ and $d_{\min}$ are maximum and minimum of $d(\mathbf{x})$. $0 < w_m < 1$ is the weight of the merit function that can either drive the search towards local minima or global exploration. For example, minimising the first and second term in Eq. 9 would suggest a candidate point located close to, and far away, from the evaluated points respectively. Following [43], the weight w_m will cycle through these four values: 0.3, 0.5, 0.7, and 0.95, to achieve a gradual transition from global search to local search.

4. The algorithm evaluates the objective function value at the candidate point, with which it updates the surrogate. This is followed by repetition between step 2 and 4 until the minimum distance between the new candidate point and its closest counterpart is less than a threshold value. Then, the algorithm will discard all previous candidate points from the surrogate, and reset the surrogate by a new round of sampling (restart from step 1). This helps in preventing the optimal solution found to be a local minimum. The entire optimisation loop stops when the terminating criterion is met. The terminating criterion could be the total number of function evaluations or total simulation time, or a combination of both. The final optimum design can then be selected by finding the minimum from all evaluated initial and candidate points.

3.2. Objective function evaluation

The objective function $f(\mathbf{x})$ is evaluated from the frequency response functions (FRFs) of the blades based on the nonlinear dynamic analysis (see section 2.2). This study is only concerned with the first flexural in-phase (IP) and out-of-phase (OOP) modes where large platform movements are expected [6]. Considering equally the contribution from both, the objective function is written as

$$f(\mathbf{x}) = 0.5g_{\mathrm{IP}}(\mathbf{x}) + 0.5g_{\mathrm{OOP}}(\mathbf{x}). \tag{10}$$

In addition to the the nominal design configuration $\mathbf{x^0}$, we consider m possible variational configurations $\mathbf{x^1}, ..., \mathbf{x^m}$ as a result of variation within manufacture tolerance. For either IP or OOP modes, the objective function is expressed as a combination of dynamic performance of nominal configuration $f_{\mathrm{dynamic}}(\mathbf{x^0})$ and the measure of robustness for all tested configurations $f_{\mathrm{robustness}}(\mathbf{x^0}, ..., \mathbf{x^m})$

$$g(\mathbf{x}) = w_f f_{\mathrm{dynamic}}(\mathbf{x^0}) + (1 - w_f) f_{\mathrm{robustness}}(\mathbf{x^0}, ..., \mathbf{x^m}) \tag{11}$$

where w_f is the weight coefficient for objective function with the extreme cases of $w_f = 0$ and $w_f = 1$ denoting dominating influence by *robustness* and *damping* respectively. The damping performance is measured as the combination of reduction of resonance amplitude and frequency shift

$$f_{\mathrm{dynamic}}(\mathbf{x^0}) = \frac{|\omega^{\mathbf{r}}_{\mathrm{l}}(\mathbf{x^0}) - \omega^{\mathbf{r}}_{\mathrm{nl}}(\mathbf{x^0})|}{\bar{\omega}_{\mathrm{tol}}\omega^{\mathbf{r}}_{\mathrm{l}}(\mathbf{x^0})} + \frac{\delta^{\mathbf{r}}_{\mathrm{nl}}(\mathbf{x^0})}{\delta^{\mathbf{r}}_{\mathrm{l}}(\mathbf{x^0})} \tag{12}$$

where δ^r and ω^r refer to resonance amplitude and frequency respectively; subscripts $_{\mathrm{l}}$ and $_{\mathrm{nl}}$ denote the cases under linear and nonlinear excitation loads respectively; $\bar{\omega}_{\mathrm{tol}}$ is the absolute percentage tolerance of the frequency shift – this is used to bring the first term in Eq. 12 up to the same magnitude (between 0 and 1) of the second term in Eq. 12. The robustness function is the summation of the coefficients of variance (standard deviation over mean) $\widehat{C_v}$ for both the resonance amplitude and frequencies under linear and nonlinear excitation loads

$$\begin{aligned} f_{\mathrm{robustness}}(\mathbf{x^0}, ..., \mathbf{x^m}) = {} & \frac{\widehat{C_v}[\omega^r_{\mathrm{l}}(\mathbf{x^0}), ..., \omega^r_{\mathrm{l}}(\mathbf{x^m})] + \widehat{C_v}[\omega^r_{\mathrm{nl}}(\mathbf{x^0}), ..., \omega^r_{\mathrm{nl}}(\mathbf{x^m})]}{\bar{\omega}_{\mathrm{tol}}} \\ & + \widehat{C_v}[\delta^r_{\mathrm{l}}(\mathbf{x^0}), ..., \delta^r_{\mathrm{l}}(\mathbf{x^m})] + \widehat{C_v}[\delta^r_{\mathrm{nl}}(\mathbf{x^0}), ..., \delta^r_{\mathrm{nl}}(\mathbf{x^m})]. \end{aligned} \tag{13}$$

4. Results and discussions

To demonstrate the efficacy of the current method, a comparison between the parametric simulation method and the proposed surrogate model will be made under the same maximum number of 216 function evaluations. The blade and damper material properties were set to mild steel (Young's modulus of 197 GPa and density of 7800 kg/m^3), and the values for the contact properties were $K_t = 6 \times 10^4$ N/mm^3, $K_n = 6 \times 10^4$ N/mm^3 and $\mu = 0.6$ for the area contact [6], and $K_t = 6 \times 10$ N/mm, $K_n = 6 \times 10$ N/mm and $\mu = 0.6$ for the line contact [40]. Following the study by Pesaresi et al. [6], two excitation forces of 0.17 and 17 N were applied to the base of one blade to excite a typical linear and nonlinear response in Eqs. 12 and 13, respectively. The first three harmonics, with the harmonic 'zero' (static term), were included in the Fourier truncated representation of the response following [6]. A weight coefficient of $w_f = 0.5$, giving equal importance to *dynamic response* and *robustness*, was chosen for Eq. 11. In Eqs. 12 and 13, an absolute percentage tolerance of the frequency shift of $\bar{\omega}_{\mathrm{tol}}$=2.5% was used as a reference value to establish the influence of resonance frequency shift. The value for $\bar{\omega}_{\mathrm{tol}}$ should be carefully chosen, since it affects the weighting of the components in the objective function, and in turn, the final optimisation design. Results that will shown later in this section (Fig. 11a) will confirm that the current value of $\bar{\omega}_{\mathrm{tol}} = 2.5\%$ is reasonable since the optimised design, with its nominal and variation configurations, all display excellent damping performance and limited frequency shift (less than 1%). The design variables were set to:

$$0.6 \leq \bar{\theta} \leq 1.2, \quad 0.8 \leq \bar{w} \leq 1.5, \quad 0.8 \leq \bar{h} \leq 1.3. \tag{14}$$

to ensure a feasible design of the damper.

The results from the parametric simulation method are shown in Fig. 7. The design space defined by Eq. 14 is filled evenly by $6 \times 6 \times 6 = 216$ configurations with the individual design variable being equally partitioned within its range. Figures 7a- 7f show the contour plot of the objective function value as a function of $\bar{\theta}$ and $\bar{w}$ for different non-dimensional values of $\bar{h}$. The colour bar indicates the contour value of the objective function with the maximum (i.e. 1.5) being the penalty for unrealistic design variables that violate the geometric constraints and the minimum being the local optimum solution (its value is clearly indicated at the lower range of the colour bar). It is unsurprising that the objective function (evaluated based on the nonlinear dynamic analysis of the blade-damper system) has a general nonlinear relationship with each design variable. In general, variations of $\bar{\theta}$ and $\bar{w}$ have a greater influence on objective function value than $\bar{h}$. F Based on the results in Figure 7, two configurations – $\bar{\theta}$=1.08, $\bar{w}$=1.08, $\bar{h}$=0.80 in Fig. 7a and $\bar{\theta}$=0.96, $\bar{w}$=1.08, $\bar{h}$=1.30 in Fig. 7f – exist that have identical minimum objective function values of 0.289 out of the 216 parametric simulations. To better understand the behaviour of these two optimal cases, the corresponding UPD design and simulated FRFs are shown in Figs. 8a and 8b. Despite identical overall objective function values, the former design has groove angle greater than the platforms, while the latter one has a smaller groove angle. This leads to two very different blade-damper interaction mechanisms, and consequently to very different simulated FRFs. In the first case the entire UPD is underneath the platform (since the UPD's groove angle is greater than that of platform $\bar{\theta} > 1$), with the lower edge of the right-hand damper side in contact with the platform, leading to a quasi-static stress concentration at the lower end of the UPD's right-hand surface. For the smaller groove angle, the stress on the right surface of the UPD concentrates at its upper end since $\bar{\theta} < 1$. Due to the nonlinear nature of the problem, very different dynamic response and robustness behaviour can be observed in Fig. 8a and 8b. The large groove angle design leads in the IP mode to a significant amount

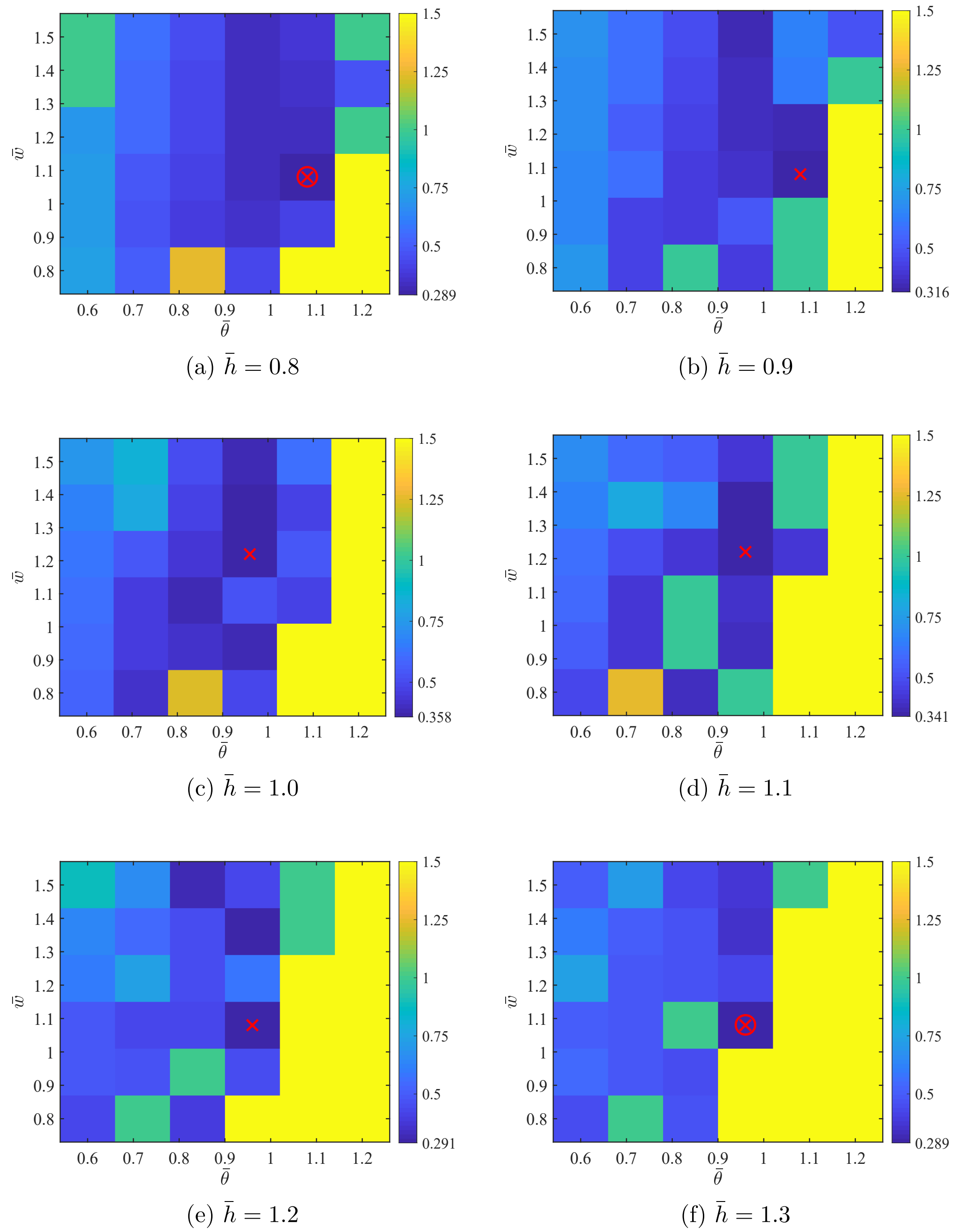

(a) $\bar{h} = 0.8$

(b) $\bar{h} = 0.9$

(c) $\bar{h} = 1.0$

(d) $\bar{h} = 1.1$

(e) $\bar{h} = 1.2$

(f) $\bar{h} = 1.3$

Figure 7: Results of parametric simulation method for different values of $\bar{\theta}$, $\bar{w}$ and $\bar{h}$. X and O denote respectively the local and global minimum location.

of damping and a small frequency shift due to higher excitation levels (solid and dotted lines), but it also shows a strong sensitivity with regards to small variations in the groove

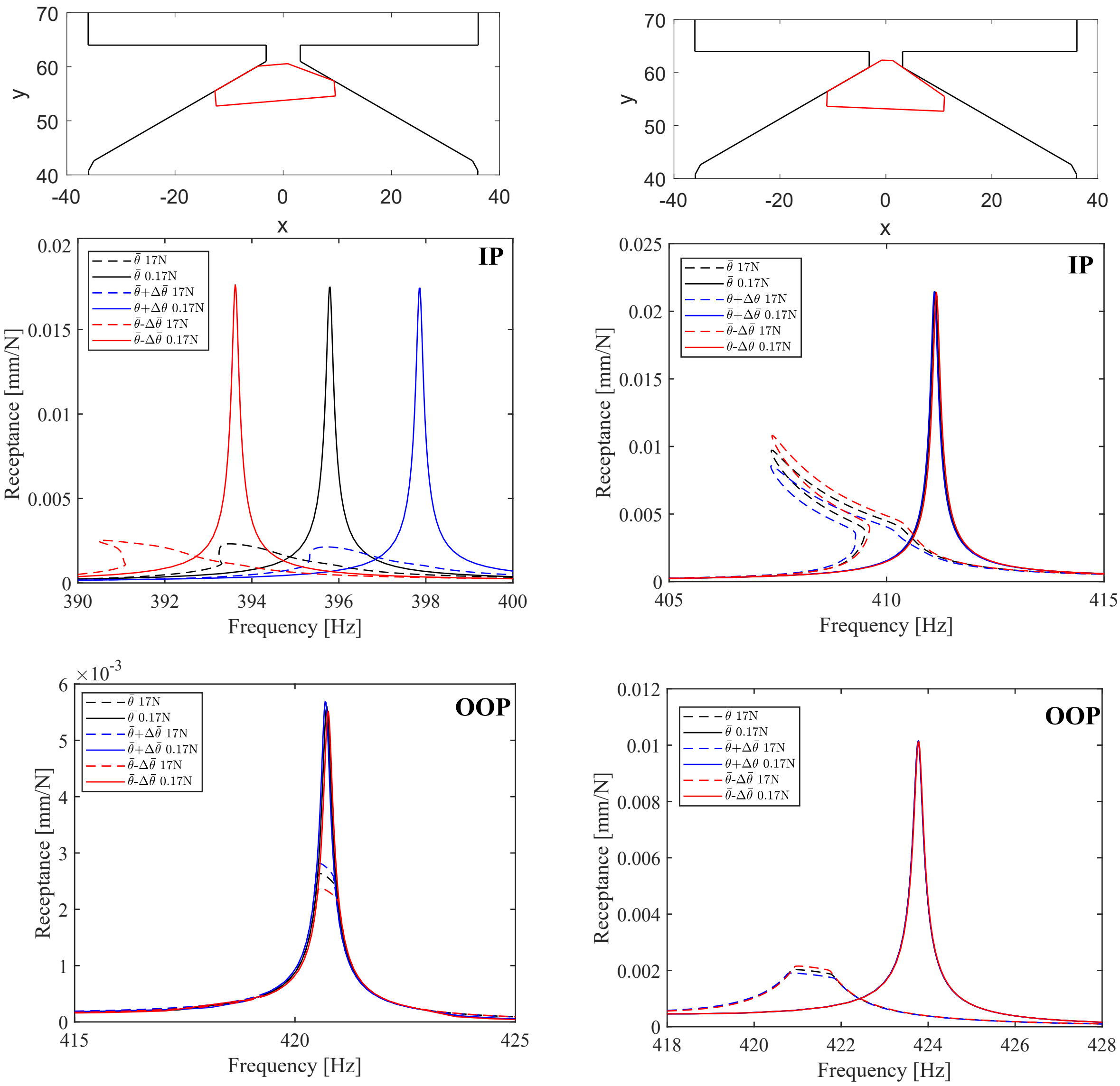

(a) $\bar{\theta}$=1.08, $\bar{w}$=1.08, $\bar{h}$=0.80 (b) $\bar{\theta}$=0.96, $\bar{w}$=1.08, $\bar{h}$=1.30

Figure 8: UPD nominal design and simulated IP and OOP FRFs for nominal and variational configurations corresponding to the local optimal solution in (a) Fig. 7a and Fig. 7f.

angle (blue and red lines). The narrow groove angle IP mode instead is relatively insensitive towards groove angle variations, but leads to less damping and a slightly larger frequency shift. The behaviour is inverted for the OOP mode, which explains why the overall objective function of the two fundamentally different damper designs lead to the same minimum value and highlights the importance of choosing the weights correctly to ensure that the optimum design displays reasonable individual performance as defined in the objective function.

Figure 9 summarises the resulting objective function for the proposed surrogate model

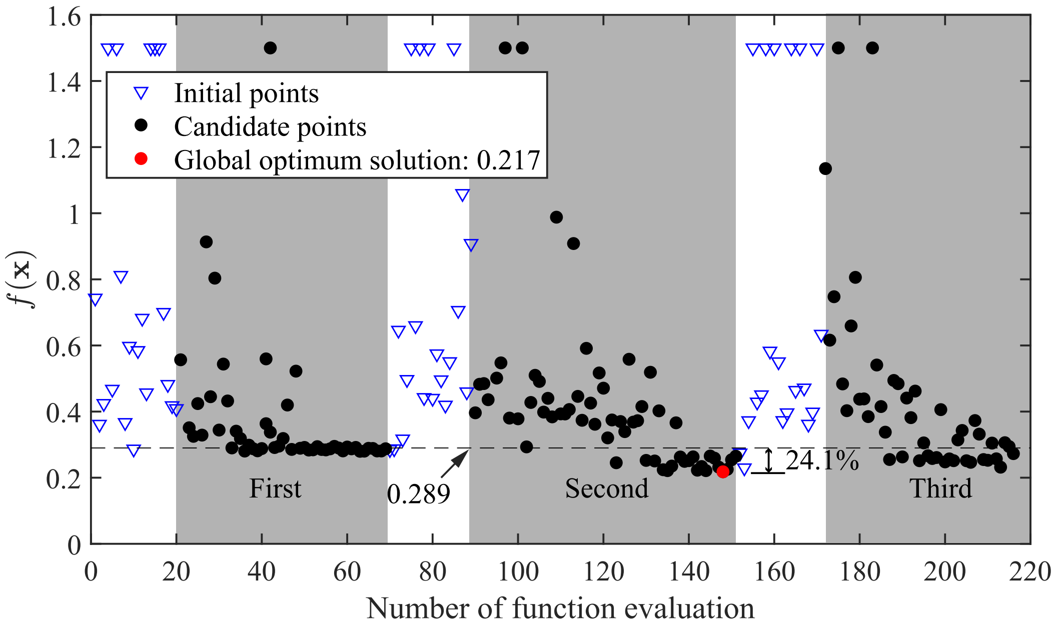

Figure 9: Trajectory of objective function value using the current surrogate model optimisation. - - - denotes the minimum solution from the parametric simulation method (see Fig. 7).

method. As previously explained, the algorithm alternates between the phase of evaluating initial points (blue triangles) and the phase of identifying and adding candidate points to the surrogate model (black dot). Three rounds of full evaluations (initial together with candidate points) were carried out within the 216 allowed iterations. The minimum objective function value from the previous parametric simulation method (0.289 in Fig. 7) is also included for comparison. The results show that the objective function value evaluated at initial points varies significantly, but once considerable candidate points are added it eventually converges towards a minimum. Interestingly in the first round of full evaluation the minimum solution is close to that from the parametric simulation method, while in the second and third iteration, lower minimum solutions were found. A close examination in Fig. 10 will show that the design configuration shown in Fig. 8a is, surprisingly, within the clustering region of the first patch of candidate points that are reaching a local minimum. Due to the stochastic nature of the surrogate method, it is not surprising to find that the objective function value for the first initial point within the third round of evaluation is very close to the optimum solution found in the previous round. The proposed surrogate model was eventually able to improve the optimal solution by 24.1% when compared to the parametric simulation, within 150 iterations, thereby providing a significantly improved solution in less than 70% of the computational effort.

To aid the interpretation of the provided results, Figure 10 shows the dispersion of the initial points and candidate points within the three-dimensional design space of $\bar{\theta} - \bar{w} - \bar{h}$ during the optimisation loop. The contour of the corresponding objective function value is

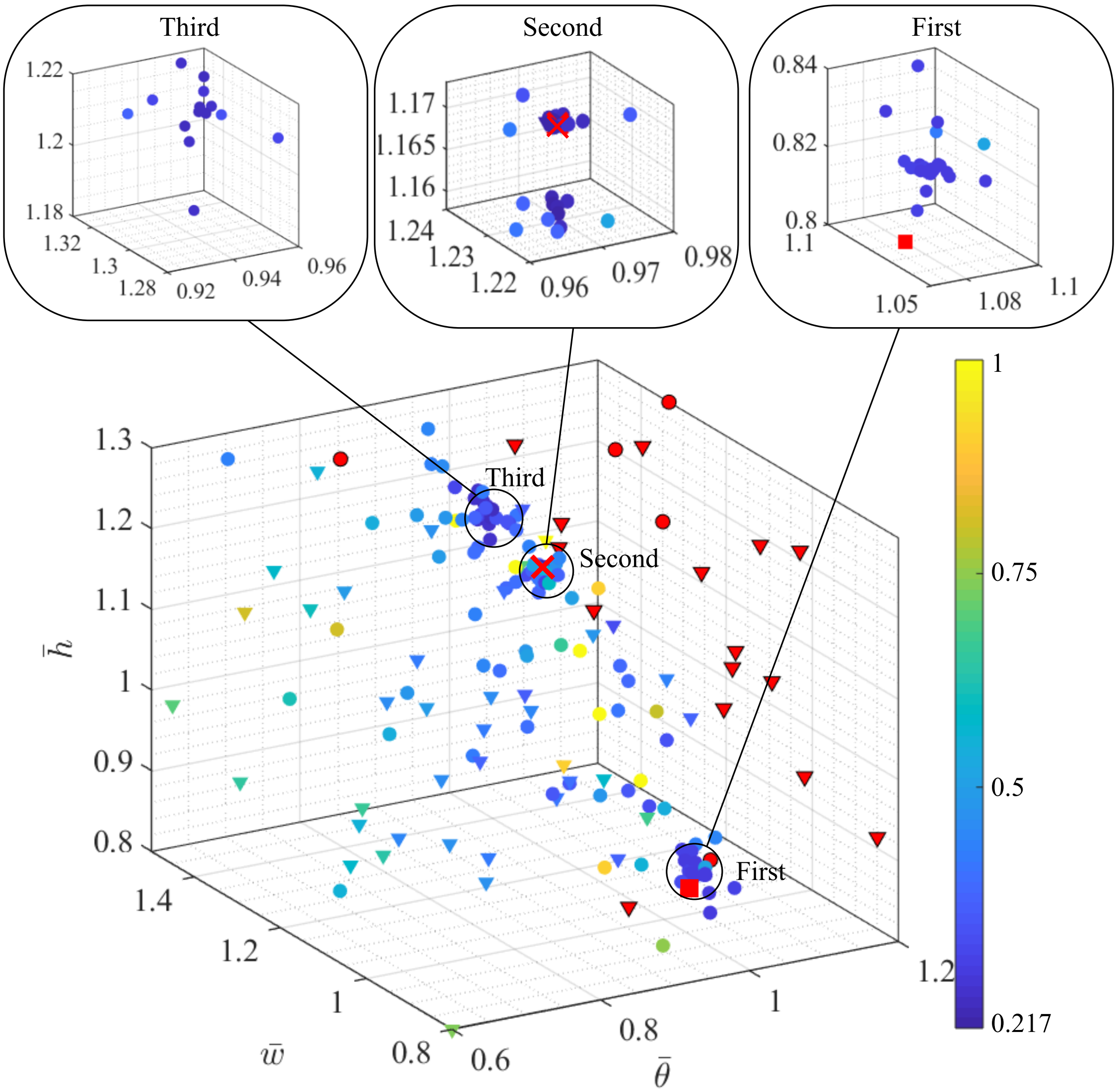

Figure 10: Contour plot of objective function solutions during the optimisation loop. ▼ refers to initial points; ● refers to candidate points; X denotes the global minimum location; ■ refers to the design configuration in Fig. 8a.

indicated on the colour bar. It can be seen that the initial points, which are based on quasi-random sequences, are uniformly distributed around the design space without clustering. This ensures the general accuracy of the surrogate model over the broad range of the design space. The infeasible UPD designs are plotted in red (a penalty of 1.5 is given), most of which are initial points. This indicates that the candidate points (which are the minimum solutions of the merit function) rarely violate the inequality conditions (Eq. 3) and the majority of the candidate points are contributing towards minimising the objective function value. A close examination of Fig. 10 reveals three sets of clustered candidate points, which respectively belong to the three round of the full evaluation in Fig. 9. The fact that the regions containing the three clustering candidate points are separated illustrates the beneficial feature of the current method to explore global minima rather than becoming 'trapped' in a local minimum.

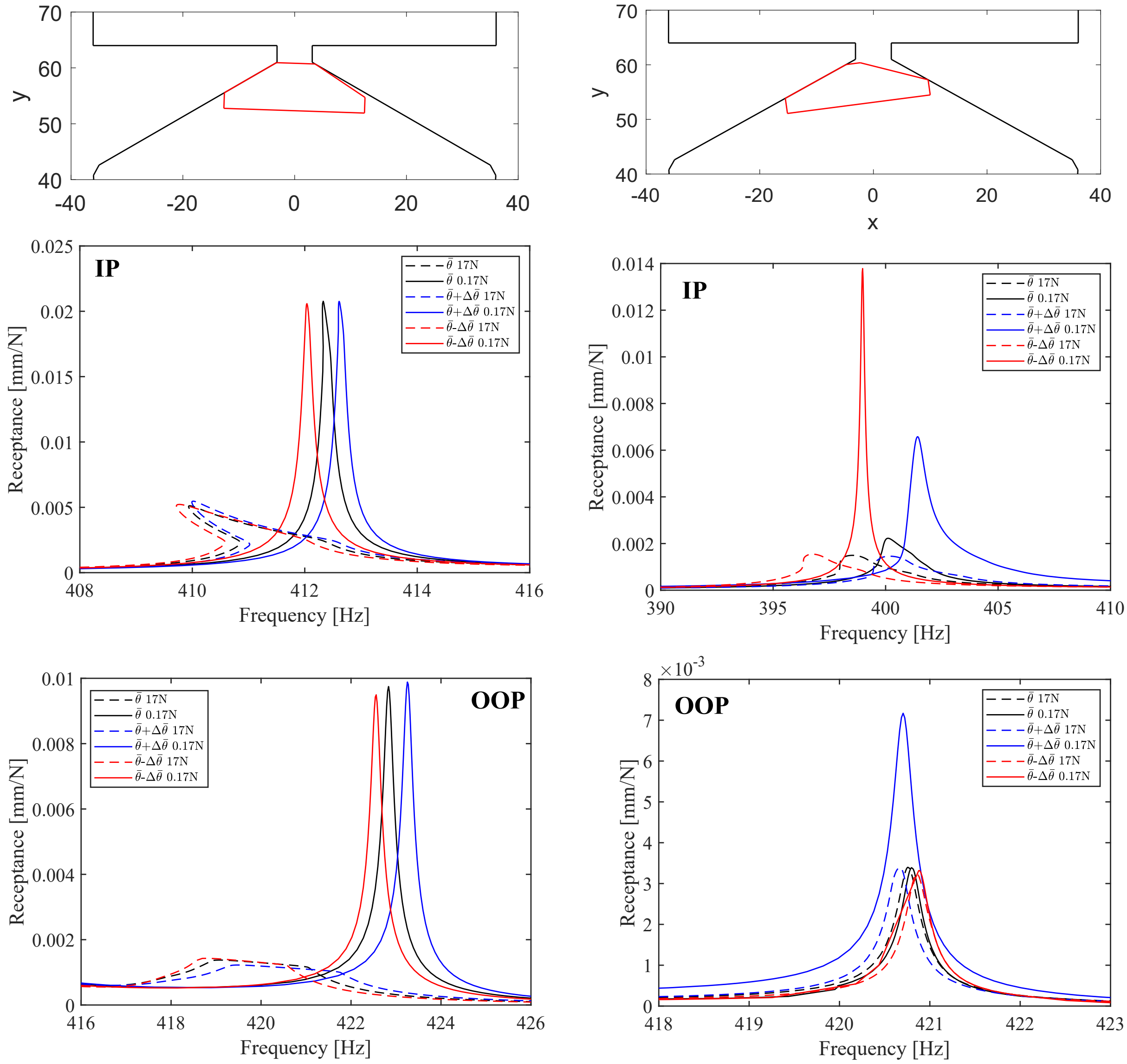

(a) $\bar{\theta}$=0.97, $\bar{w}$=1.23, $\bar{h}$=1.17 (b) $\bar{\theta}$=1.13, $\bar{w}$=1.24, $\bar{h}$=0.96

Figure 11: UPD nominal design and simulated IP and OOP FRFs for nominal and variational configurations corresponding to (a) the global optimal solution and (b) an example for poor robustness in Fig. 10.

The UPD design and simulation results for the global optimum configuration in the surrogate model optimisation (Figs. 9 and 10) are shown in Fig. 11a. The design configuration is similar to that shown earlier in Fig. 8b, where quasi-static stress concentrates on the upper end of right-hand UPD surface. The improvement of objective function value is largely due to the further reduction of resonance amplitude in the IP mode since other performance (robustness, frequency shift and damping performance in OOP mode) are relatively close when comparing Fig. 11a and Fig. 8b. Figure 11b presents an example of how sensitive the nonlinear dynamic response of the blade-damper system could be over only a slight change of design variable (i.e. $\pm 2°$ on groove angle). In IP and OOP modes, the FRF curves under either low or high excitation loads, vary considerably for the nominal and variational configurations. This highlights the importance to consider the manufacture tolerances on geometrical properties when carrying out optimisation study on UPD design.

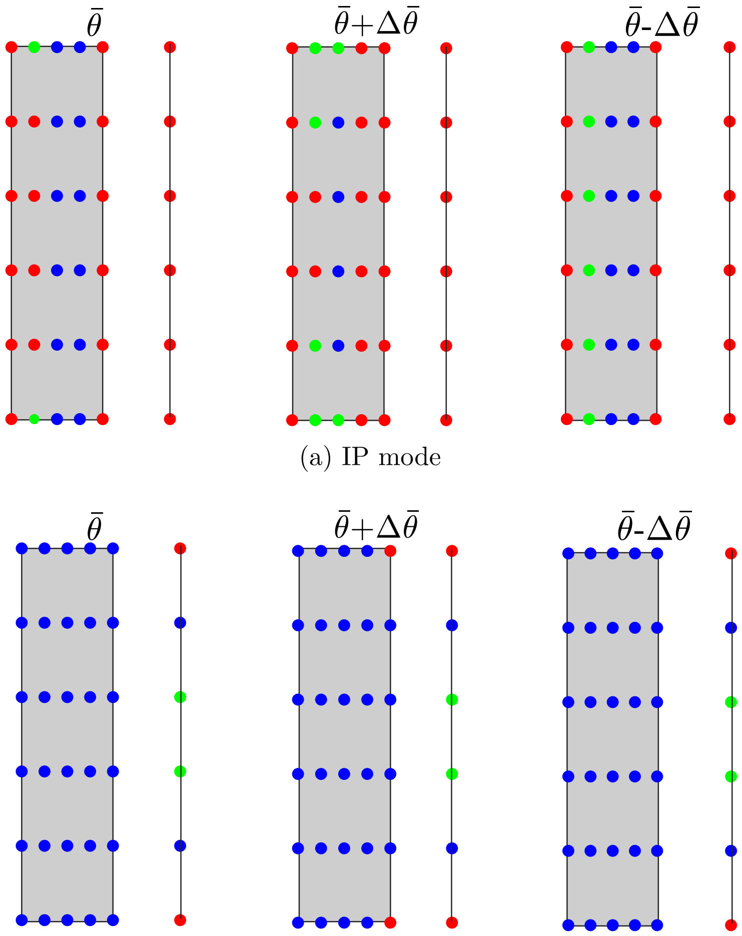

(a) IP mode

(b) OOP mode

Figure 12: Contact conditions for each contact node at the damper interface under 17 N at resonance frequencies for the simulations given in Fig. 11a. ● stuck; ● slip; ● slip-separation; ● gap.

To provide further insights on the local contact dynamics that drives the good and robust performance of the optimum design in Fig. 11a, Figure 12 shows the contact conditions at the IP and OOP modes under high excitation load (17 N) at resonance frequencies. The explicit damper model developed in [6] permits the identification of four different contact behaviours at the interface for the contact node during a vibration cycle: stuck condition where linear

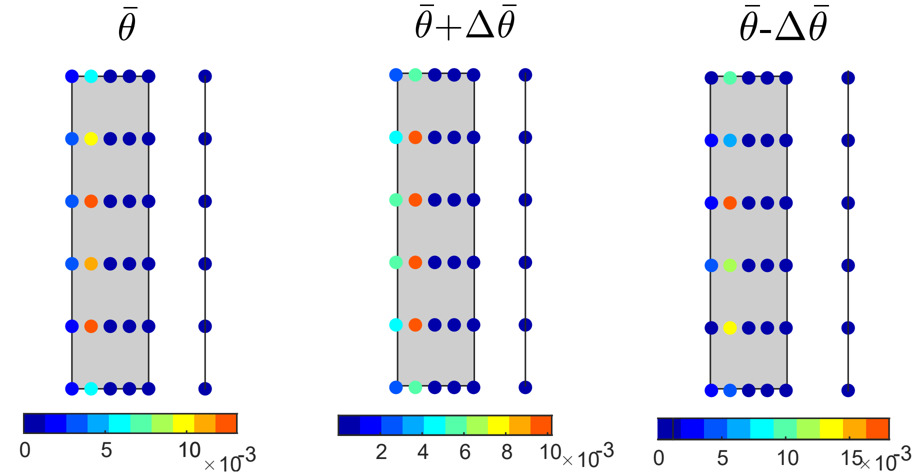

(a) IP mode

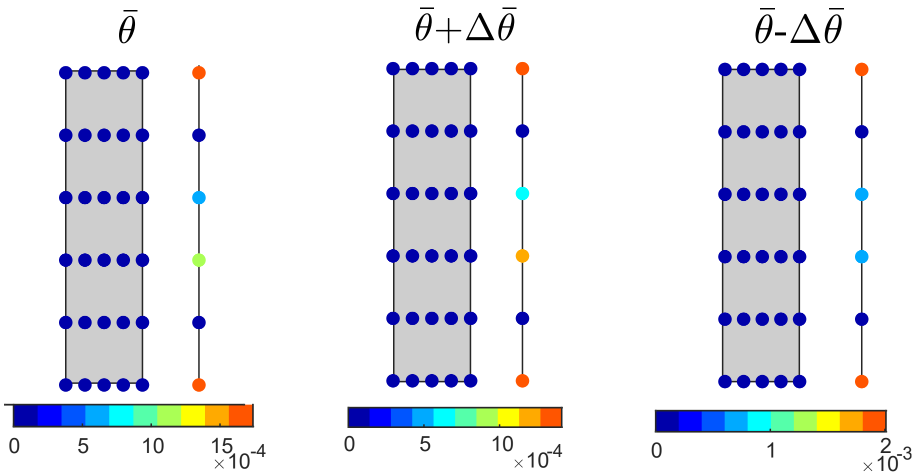

(b) OOP mode

Figure 13: Energy dissipation for each contact node at the damper interface under 17 N at resonance frequencies for the simulations given in Fig. 11a.

nodes do not dissipate energy (blue dots), stick-slip transition which is beneficial for energy dissipation (green dots), slip-separation transition (red dots) and separation (cyan dots). The contact conditions under low excitation load (0.17 N) are excluded here purposefully since they are all under stuck condition at low excitation forces. It can be seen that the contact conditions for nominal and variational configurations are consistent in both IP and OOP mode. In IP mode the central region of the left surface of the UPD stays stuck even at high excitation load whereas the nodes adjacent to the boundary mostly slip (green dots) or slip and separates (red dots) - this is in line with the findings in [6]. In OOP mode the entire left surfaces stay stuck during the vibration cycle, despite the high excitation load. Results of energy dissipation for each contact node is shown in Fig. 13. It reveals that the dry friction from left and right side of the UPD always dissipate energy in IP and OOP mode respectively. This explains the robust and significant reduction of resonance amplitude in both modes for the nominal and variational UPDs, as seen in Fig. 11a.

5. Conclusions

An optimisation framework for the robust design of an underplatform damper (UPD) with dry friction interfaces was developed. The approach combines high-order nonlinear dynamic models of the damper with surrogate model optimisation to provide good damping coupled with stable resonance frequency behaviour and small response variations due to manufacturing tolerances. It was shown that the nonlinear dynamic response of the blade-damper system can be extremely sensitive to a slight change of geometric properties; and hence it is important to consider geometric uncertainty when optimising UPD. Comparison between the proposed surrogate model and the conventional parametric simulation method has been made, where the current method is shown to be more computational cost-efficient to find a considerably improved optimum solution. The close examinations of the contact condition and energy dissipation at the blade-damper interface reveal that the global optimum design proposed by the surrogate model is effective in dissipating energy through slipping in both the IP and OOP mode.

Acknowledgment

The authors would like to thank Innovate UK and the ATI for supporting this research as part of the MALIT programme.

References

[1] Gastaldi, C., Berruti, T. M., Gola, M. M., The Relevance of Damper Pre-Optimization and Its Effectiveness on the Forced Response of Blades, Journal of Engineering for Gas Turbines and Power 140 (6) (2018) 062505–062505–11.

[2] Gastaldi, C., Gola, M. M., Pre-optimization of Asymmetrical Underplatform Dampers, Journal of Engineering for Gas Turbines and Power 139 (1) (2017) 012504.

[3] Griffin, J. H., A Review of Friction Damping of Turbine Blade Vibration, International Journal of Turbo and Jet Engines 7 (3-4) (1990) 297–308.

[4] Petrov, E. P., Explicit Finite Element Models of Friction Dampers in Forced Response Analysis of Bladed Disks, J. Eng. Gas Turbines Power 130 (2) (2008) 022502–022502–11.

[5] Cameron, T. M., Griffin, J. H., Kielb, R. E., Hoosac, T. M., An Integrated Approach for Friction Damper Design, J. Vib. Acoust. 112 (2) (1990) 175–182.

[6] Pesaresi, L., Salles, L., Jones, A., Green, J., Schwingshackl, C., Modelling the nonlinear behaviour of an underplatform damper test rig for turbine applications, Mech. Syst. Sig. Process. 85 (2017) 662–679.

[7] Schwingshackl, C., Petrov, E., Ewins, D., Measured and estimated friction interface parameters in a nonlinear dynamic analysis, Mech. Syst. Sig. Process. 28 (2012) 574–584.

[8] Csaba, G., Forced response analysis in time and frequency domains of a tuned bladed disk with friction dampers, J. Sound Vib. 214 (3) (1998) 395–412.

[9] Firrone, C. M., Zucca, S., Gola, M. M., The effect of underplatform dampers on the forced response of bladed disks by a coupled static/dynamic harmonic balance method, Int. J. Non Linear Mech. 46 (2) (2011) 363–375.

[10] Petrov, E. P., A High-Accuracy Model Reduction for Analysis of Nonlinear Vibrations in Structures With Contact Interfaces, J. Eng. Gas Turbines Power 133 (10) (2011) 102503–102503–10.

[11] Petrov, E. P., Ewins, D. J., Advanced Modeling of Underplatform Friction Dampers for Analysis of Bladed Disk Vibration, J. Turbomach. 129 (1) (2006) 143–150.

[12] Petrov, E. P., Ewins, D. J., Analytical Formulation of Friction Interface Elements for Analysis of Nonlinear Multi-Harmonic Vibrations of Bladed Disks, J. Turbomach. 125 (2) (2003) 364–371.

[13] Zucca, S., Firrone, C. M., Gola, M., Modeling underplatform dampers for turbine blades: a refined approach in the frequency domain, J. Vib. Control 19 (7) (2013) 1087–1102.

[14] Krack, M., Salles, L., Thouverez, F., Vibration prediction of bladed disks coupled by friction joints, Arch. Comput. Methods Eng. 24 (3) (2017) 589–636.

[15] Peter, S., Scheel, M., Krack, M., Leine, R. I., Synthesis of nonlinear frequency responses with experimentally extracted nonlinear modes, Mech. Syst. Sig. Process. 101 (2018) 498–515.

[16] Grolet, A., Thouverez, F., On a new harmonic selection technique for harmonic balance method, Mech. Syst. Sig. Process. 30 (2012) 43–60.

[17] Yuan, J., El-Haddad, F., Salles, L., Wong, C., Numerical Assessment of Reduced Order Modeling Techniques for Dynamic Analysis of Jointed Structures With Contact Nonlinearities, J. Eng. Gas Turbines Power 141 (3) (2018) 031027–031027–12.

[18] Nguyen, A.-T., Reiter, S., Rigo, P., A review on simulation-based optimization methods applied to building performance analysis, Appl. Energy 113 (2014) 1043–1058.

[19] Petrov, E. P., Direct Parametric Analysis of Resonance Regimes for Nonlinear Vibrations of Bladed Disks, J. Turbomach. 129 (3) (2006) 495–502.

[20] Krack, M., Tatzko, S., Panning-von Scheidt, L., Wallaschek, J., Reliability optimization of friction-damped systems using nonlinear modes, J. Sound Vib. 333 (13) (2014) 2699–2712.

[21] Tang, W., Epureanu, B. I., Geometric optimization of dry friction ring dampers, Int. J. Non Linear Mech. 109 (2019) 40–49.

[22] Panning, L., Sextro, W., Popp, K., Optimization of the Contact Geometry Between Turbine Blades and Underplatform Dampers With Respect to Friction Damping, ASME Turbo Expo 2002: Power for Land, Sea, and Air (2002) 991–1002.

[23] Gosavi, A., Simulation-based optimization : parametric optimization techniques and reinforcement learning, Kluwer Academic Publishers, Boston, Mass. ; London, 2003.

[24] Koziel, S., Leifsson, L. (Eds.), Surrogate-based modeling and optimization: applications in engineering, 1st Edition, New York: Springer, New York, 2013.

[25] Chakraborty, S., Goswami, S., Rabczuk, T., A surrogate assisted adaptive framework for robust topology optimization, Comput. Methods Appl. Mech. Eng. 346 (2019) 63–84.

[26] Forrester, A. I. J., Sbester, A., Keane, A. J., Engineering Design via Surrogate Modelling, John Wiley & Sons, Ltd, Chichester, UK, 2008.
URL http://doi.wiley.com/10.1002/9780470770801

[27] Qiu, N., Gao, Y., Fang, J., Sun, G., Li, Q., Kim, N. H., Crashworthiness optimization with uncertainty from surrogate model and numerical error, Thin-Walled Structures 129 (2018) 457–472.

[28] Müller, J., Shoemaker, C. A., Piché, R., SO-MI: A surrogate model algorithm for computationally expensive nonlinear mixed-integer black-box global optimization problems, Computers & Operations Research 40 (5) (2013) 1383–1400.

[29] Jones, D. R., A Taxonomy of Global Optimization Methods Based on Response Surfaces, J. Global Optim. 21 (2001) 345–383.

[30] Li, M., Wang, Z., Surrogate model uncertainty quantification for reliability-based design optimization, Reliability Engineering & System Safety.

[31] Voutchkov, I., Keane, A., Multi-Objective Optimization Using Surrogates, in: Tenne, Y., Goh, C.-K. (Eds.), Computational Intelligence in Optimization: Applications and Implementations, Springer Berlin Heidelberg, Berlin, Heidelberg, 2010, pp. 155–175.
URL https://doi.org/10.1007/978-3-642-12775-5_7

[32] Myers, R., Montgomery, D. C., Response Surface Methodology, Process and Product Optimization

using Designed Experiments, London: Wiley, 1995.

[33] Friedman, J. H., Multivariate adaptive regression splines, The Annals of Statistics 19 (1) (1991) 1–141.

[34] Gutmann, H.-M., A Radial Basis Function Method for Global Optimization, J. Global Optim. 19 (3) (2001) 201–227.

[35] Lam, X. B., Kim, Y. S., Hoang, A. D., Park, C. W., Coupled aerostructural design optimization using the kriging model and integrated multiobjective optimization algorithm, Journal of Optimization Theory and Applications 142 (3) (2009) 533–556.

[36] Culla, A., Massi, F., Uncertainty model for contact instability prediction, The Journal of the Acoustical Society of America 126 (3) (2009) 1111–1119.

[37] Grange, P., Clair, D., Baillet, L., Fogli, M., Brake squeal analysis by coupling spectral linearization and modal identification methods, Mech. Syst. Sig. Process. 23 (8) (2009) 2575–2589.

[38] Gaul, L., Nitsche, R., The role of friction in mechanical joints, Appl. Mech. Rev. 54 (2) (2001) 93–106.

[39] Fantetti, A., Gastaldi, C., Berruti, T. M., Modeling and testing friction flexible dampers: Challenges and peculiarities, Exp. Tech. 42 (4) (2018) 407–419.

[40] Fantetti, A., Tamatam, L., Volvert, M., Lawal, I., Liu, L., Salles, L., Brake, M., Schwingshackl, C., Nowell, D., The impact of fretting wear on structural dynamics: Experiment and simulation, Tribology International 138 (2019) 111 – 124.

[41] Petrov, E. P., A Method for Use of Cyclic Symmetry Properties in Analysis of Nonlinear Multiharmonic Vibrations of Bladed Disks, J. Turbomach. 126 (1) (2004) 175.

[42] Petrov, E. P., Explicit Finite Element Models of Friction Dampers in Forced Response Analysis of Bladed Disks, J. Eng. Gas Turbines Power 130 (2) (2008) 022502–022502–11.

[43] Regis, R. G., Shoemaker, C. A., A Stochastic Radial Basis Function Method for the Global Optimization of Expensive Functions, INFORMS Journal on Computing 19 (4) (2007) 497–509.

[44] Powell, M. J. D., The theory of radial basis function approximation in 1990, Advances in numerical analysis (1992) 105–210.